

Optical Nuclei of Radio-loud AGN and the Fanaroff-Riley Divide

P. Kharb and P. Shastri

Indian Institute of Astrophysics, Koramangala, Bangalore - 560 034, India

Abstract. We investigate the nature of the point-like optical “cores” that have been found in the centres of the host galaxies of a majority of radio galaxies by the *Hubble Space Telescope*. We examine the evidence that these optical cores are relativistically beamed, and look for differences in the behaviour of the cores found in radio galaxies of the two Fanaroff-Riley types. We also attempt to relate this behaviour to the properties of the optical nuclei in their highly beamed counterparts (the BL Lac objects and radio-loud quasars) as hypothesized by the simple Unified Scheme. Simple model-fitting of the data suggests that the emission may be coming from a non-thermal relativistic jet. It is also suggestive that the contribution from an accretion disk is not significant for the FRI objects and for the narrow-line radio galaxies of FRII type, while it may be significant for the Broad-line objects, and consistent with the idea that the FRII optical cores seem to suffer from extinction due to an obscuring torus while the FRI optical cores do not. These results are in agreement with the Unified Scheme for radio-loud AGNs.

Key words. galaxies: active – BL Lacertae objects: general – galaxies: nuclei – quasars: general

1. Introduction

‘Radio-loud’ Active Galactic Nuclei (AGNs) include radio galaxies, BL Lac objects and quasars. They show twin lobes of synchrotron-emitting plasma connected to a ‘core’ by plasma jets on scales of ~ 100 kpc, the core being coincident with the centre of an elliptical galaxy. Fanaroff & Riley (1974) recognised that the radio morphology of radio galaxies along with their total radio power fell in two distinct subclasses: the lower-power Fanaroff-Riley type I (FRI) objects showed extended plumes and tails with no distinct termination of the jet while the higher-power type II (FRII) objects showed narrow, collimated jets and terminal “hot spots”. The total radio luminosity break at 178 MHz occurred at $L_{178} \approx 2 \times 10^{25} \text{ W Hz}^{-1}$ (for $H_0 = 50 \text{ km s}^{-1} \text{ Mpc}^{-1}$, $q_0 = 0$) although at higher frequencies the break is less sharp (Urry & Padovani 1995).

The FRII radio galaxies also have systematically more luminous optical emission lines (Zirbel & Baum 1995) while FRI radio galaxies inhabit richer environments (Prestage & Peacock 1988); the value of the FRI/FRII radio luminosity break increases with the optical luminosity of the host galaxy (Ledlow & Owen 1996). The origin of the F–R dichotomy is far from clear; some suggested possibilities have been differences in the spin of the supermassive black hole resulting in different jet kinetic powers (Baum et al. 1995; Meier 1999), galaxy environments (Smith & Heckman 1990), and accretion rates (Baum et al. 1995). The F–R dichotomy issue is complicated by the observations of radio sources having both FRI and FRII characteristics (e.g., Capetti et al. 1995).

AGN jets experience bulk relativistic motion (Blandford & Konigl 1979) resulting in orientation playing a dominant role in their appearance. Based on orientation-independent parameters, a simple Unified Scheme (US) has emerged (Barthel 1989; Antonucci 1993; Urry & Padovani 1995), according to which the BL Lac objects and radio-powerful quasars are the likely relativistically beamed counterparts of FRI and FRII radio galaxies, respectively. The US predicts that FRI and FRII jets should have bulk relativistic motion similar to that observed in BL Lacs and quasars. The US also requires a ubiquitous optically thick torus in the FRII class of objects (*i.e.*, FRII radio galaxies and radio-loud quasars) which hides the powerful optical continuum and broad emission lines from the nucleus in the edge-on objects. No such torus is required by the US for the FRI class of objects as emission lines are either absent or very weak, and it has not been clear whether or not a torus exists.

The beamed synchrotron emission from the base of the jet or the ‘core’ must extend to visible wavelengths and there is strong evidence for it in BL Lacs and quasars (Impey & Tapia 1990; Wills et al. 1992). Recently, evidence

for an optical synchrotron component in the relatively unbeamed radio galaxies has also surfaced, in the form of unresolved nuclear sources in the high resolution galaxy images with the *Hubble Space Telescope (HST)* (e.g., Chiaberge et al. 1999, 2002; Verdoes Kleijn et al. 2002). These authors argue on the basis of the strong connection with the radio core emission, anisotropy (Capetti & Celotti 1999) and colour information that these optical cores are indeed optical synchrotron radiation.

In this paper, we further test the idea that the unresolved nuclear optical emission from radio galaxies is beamed synchrotron emission from the base of the jet, using the radio core prominence parameter (R_c) as an indicator of the orientation of the AGN axis. We then attempt to place these correlations in the broader framework of the Unified Scheme and test for consistencies. We come up with a model-fitting approach to investigate quantitatively the dependence of the optical emission on orientation and further test the predictions of the Unified Scheme in terms of the presence (or absence) of obscuring tori and the contribution of thermal accretion disks. We attempt to apply this to the available data and present the results. We further outline the caveats with our current sample and attempt to address them. The outline of the paper is as follows. In §2 we discuss the optical nuclei in FRI and FRII radio galaxies and the correlations with R_c . In §3 we compare these optical nuclei to those from BL Lacs and quasars and discuss the results along with model-fitting. §4 and 5 include the discussion and conclusions. Throughout this paper, $H_0 = 75 \text{ km s}^{-1} \text{ Mpc}^{-1}$ and $q_0 = 0.5$ have been adopted and the spectral index α is defined such that $F_\nu = \nu^{-\alpha}$.

2. The optical nuclei in FRI and FRII radio galaxies

Optical nuclei have been detected in a majority of 3CR, B2 and UGC FRI and FRII radio galaxies with the WFPC2 on board the *HST*. They appear as unresolved sources with angular sizes $\sim 0''.1$ (the PSF of the *HST*). The results of studies based on this discovery have been presented by Chiaberge et al. (1999); Capetti & Celotti (1999); Hardcastle & Worrall (2000); Capetti et al. (2002); Chiaberge et al. (2002); Verdoes Kleijn et al. (2002).

For our study we chose an eclectic sample of FRI and FRII radio galaxies with either such a detected optical nucleus or with an upper limit to its optical flux density from the above-mentioned papers. Our set of FRI radio galaxies comprise of 25 3CR (Chiaberge et al. 1999), 17 B2 (Capetti et al. 2002) and 10 UGC FRIs (Verdoes Kleijn et al. 2002) along with NGC 7052 and NGC 6251 from Capetti & Celotti (1999) and Hardcastle & Worrall (1999) respectively. Objects with ambiguous (e.g., FRI/II) morphologies are excluded. So is 3C 386 whose optical “nucleus” is in fact a foreground star (Chiaberge et al. 2002). We thus have 54 FRI radio galaxies spanning a redshift range of $0.0037 \leq z \leq 0.29$. The set of FRII radio galaxies include 53 objects from the 3CR sample presented in Chiaberge et al. (2002) and 2 B2 FRIIs from Capetti et al. (2002). Among the 55 FRIIs considered, there are 42 narrow-line radio galaxies (NLRGs) and 13 broad-line radio galaxies (BLRGs). The FRII radio galaxies span a redshift range of $0.025 \leq z \leq 0.296$.

Tables 1 and 2 list the FRI and FRII radio galaxies respectively, along with their optical and radio data. Col. (1) lists the IAU name (B1950); Col. (2) Alternate name; Col. (3) Redshift (from the references for radio core data, except for UGC FRIs which are from NED); Col. (4) dust disk minor-to-major axis ratio (superscripts ‘d’ and ‘l’ stand for disks and lanes respectively) from Verdoes Kleijn et al. (1999) except 3C 83.1, 3C 296, 3C 449, 3C 465, 3C 326 and 3C 452 which are from de Koff et al. (2000); Col. (5) logarithm of extended radio luminosity at 1.4 GHz in W Hz^{-1} , calculated using the difference between total and core flux density; data at 5 GHz was converted to 1.4 GHz using $\alpha_{radio}^{ext} = 0.7$ for extended radio emission; Col. (6) 5 GHz radio core flux density in mJy; Col. (7) reference for the radio core (and total flux density if different); Col. (8) logarithm of radio core prominence standardized to an emitted wavelength of 6 cm; Col. (9) optical core luminosity in W Hz^{-1} estimated at an emitted wavelength of 5500 Å; Col. (10) reference for optical core flux density/luminosity.

2.1. The correlations with radio core prominence for radio galaxies

The radio core prominence parameter R_c , which is the ratio of the core to extended radio flux density ($R_c \equiv S_{core}/S_{ext}$) is a known statistical indicator of orientation (Kapahi & Saikia 1982; Orr & Browne 1982) assuming that the core is the unresolved relativistically beamed nuclear jet and the lobes are unbeamed. R_c has indeed been shown to correlate with other orientation-dependent properties both in FRIIs (Kapahi & Saikia 1982) and FRIs (Laing et al. 1999). We use the parameter R_c to test if the luminosity of the optical nuclei is orientation-dependent. If the intrinsic optical synchrotron emission from the jet L_{jet}^{int} , is relativistically beamed by the Doppler factor δ where $\delta \equiv [\gamma(1 - \beta \cos\theta)]^{-1}$, β being the bulk velocity in units of the speed of light and θ is the angle between the radio axis and our line of sight, then the luminosity of the optical nuclei (L_o) should correlate with R_c .

The optical luminosities of the unresolved *HST* nuclei were K -corrected and calculated at an emitted wavelength of 5500 Å, assuming an optical spectral index $\alpha_{opt} = 1$. The radio core prominence was calculated using observed radio core and total flux densities at 5 GHz and was further K -corrected to an emitted frequency of 5 GHz. For some sources flux densities were estimated from 1.4 GHz assuming $\alpha_{radio}^{ext} = 0.7$ and $\alpha_{radio}^{core} = 0$ for the extended and core

radio emission, respectively. In Fig. 1 we plot the luminosity of the optical nuclei versus the radio core prominence for the FRI and FRII radio galaxies.

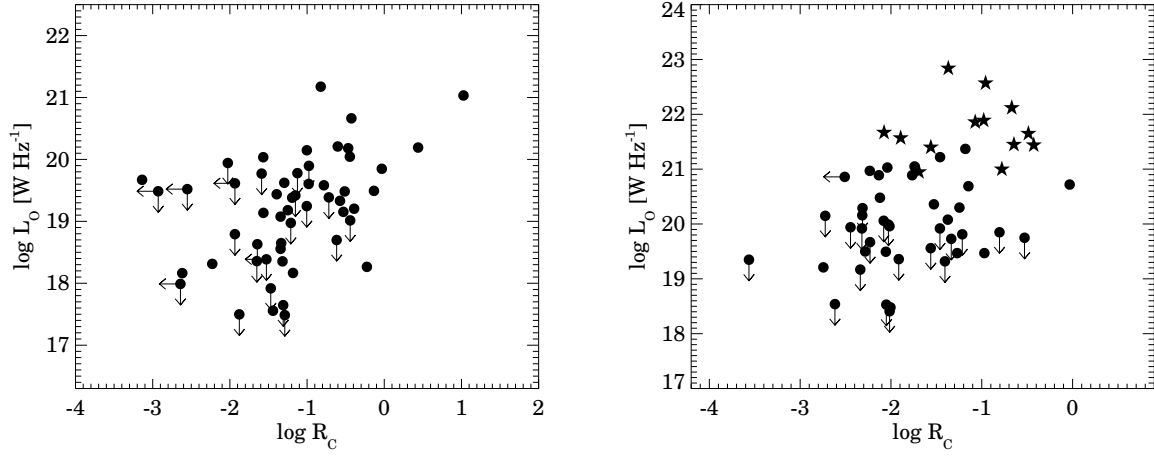


Fig. 1. The luminosity of the optical nuclei L_o , plotted against the radio core prominence R_c , for the FRI (left) and FRII radio galaxies (right). • denote radio galaxies, ★ are BLRGs, ↓ and ← denote upper limits. Statistics for the fits are listed in Table 5.

We note that there are many upper limits to nuclear optical luminosities. We have analysed the statistical significance of the correlations with the aid of the Astronomical Survival Analysis (ASURV) package as implemented in IRAF, which takes into account data which are only upper/lower limits. $\log L_o$ turns out to be significantly correlated with $\log R_c$ for the FRI radio galaxies ($p = 0.0001$, generalized Spearman Rank test, see Table 5), arguing that the nuclear optical emission is orientation-dependent in the same sense as the radio emission and may also originate in the relativistic jet and be likewise beamed.

For the FRII radio galaxies, the correlation is significant *only with the inclusion of the broad-line radio galaxies* (plotted as stars in the figure), while the narrow-line objects do not show a significant correlation by themselves ($p > 0.2$, generalized Spearman Rank test). The narrow-line FRII galaxies, show no correlation even with the more sensitive parametric Pearson's correlation test which however uses uncensored data ($p > 0.1$). This lack of correlation could be explained by the presence of a dusty obscuring torus that is hypothesized by the Unified Scheme, which could also result in many limits.

We note that the implication of the above result for the FRIs is consistent with what Verdoes Kleijn et al. (2002) suggest for their UGC FRI sample, *viz.*, that beaming also plays a role in the variance of optical luminosity of the nuclei L_o , in addition to the intrinsic variance in the nuclear jet L_{jet}^{int} , which presumably ionizes the line-emitting gas.

2.2. Kpc-scale dust disks in FRI radio galaxies

While the evidence for an obscuring torus in FRIs is thus far meagre, much larger dust disks and lanes of sizes varying from a few 100 pc to a few kpc have been discovered in many FRI radio galaxies (e.g., Verdoes Kleijn et al. 1999; de Koff et al. 2000). It has been suggested by Verdoes Kleijn et al. (1999); Capetti & Celotti (1999) and de Koff et al. (2000) that the kpc-scale radio jet tends to align with the axis of this disk. We investigate this question here for the subset of objects where data on this disk, as well as L_o and R_c are available. The results of the statistical tests are given in Table 5. We find different relations of the minor-to-major-axis ratio, b/a of the extended dust disk with nuclear optical luminosity and radio core prominence for the samples presented in the above papers. b/a of the extended dust disk correlates significantly both with the nuclear optical luminosity and radio core prominence for the de Koff et al. FRI galaxies. b/a correlates significantly with L_o for the Verdoes Kleijn et al. FRI sources only when both disks and lanes are considered together. However they show no correlation with radio core prominence. When all the objects are taken together and both dust disks and lanes are considered, b/a correlates with nuclear optical luminosity but not with radio core prominence (see Fig. 2).

It thus appears that the axes of the extended dust disks do not tend to be aligned with the orientation of the AGN, but that these disks could be causing some extinction of the flux density of the optical nuclei in FRI radio galaxies. This extinction would of course contribute to the scatter in the $L_o - R_c$ correlation.

Table 1. The FRI radio galaxies.

IAU name	Alternate name	Redshift <i>z</i>	<i>b/a</i>	$\log L_{ext}$ W Hz $^{-1}$	S_c (5 GHz) mJy	ref.	$\log R_c$	$\log L_o$ W Hz $^{-1}$	ref.
0036+030	NGC 193	0.0144	0.18 ^{<i>l</i>}	22.60	40.0	6,15	-1.31	18.35	5
0053+261	3C 28	0.1952	...	25.42	<0.2	1,3	<-2.92	<19.48	1
0055-016	3C 29	0.0448	...	25.29	93.0	1,3	-1.39	19.43	1
0055+265	4C 26.03	0.0472	...	24.61	9.0	2	-1.93	<18.54	2
0055+300	NGC 315	0.0167	0.23 ^{<i>d</i>}	24.01	617.6	2	-0.39	19.19	5
0104+321	3C 31	0.0169	0.77 ^{<i>d</i>}	24.40	92.0	1,3	-1.34	19.08	5
0120+329	NGC 507	0.0164	...	22.29	1.5	2	-1.30	<17.64	2
0123-016	3C 40	0.0180	0.91 ^{<i>d</i>}	22.17	67.8	10	-1.64	<18.63	5
0153+053	NGC 741	0.0185	...	22.75	6.0	11	-1.65	<18.35	5
0220+427	3C 66B	0.0215	0.98 ^{<i>d</i>}	24.86	182.0	1,3	-1.29	19.62	5
0305+039	3C 78	0.0288	...	24.96	964.0	1,3	-0.42	20.66	1
0318+415	3C 83.1	0.0251	0.09 ^{<i>d</i>}	24.98	21.0	1,3	-2.22	18.31	1
0316+413	3C 84	0.0176	...	24.73	42370.0	1,3	1.02	21.03	1
0331-013	3C 89	0.1386	...	25.80	49.0	1,3	-1.21	<18.97	1
0705+486	NGC 2329	0.0193	0.68 ^{<i>d</i>}	23.02	69.0	11	-0.44	20.04	5
0755+379	3C 189	0.0413	...	24.43	228.8	2	-0.46	20.18	2
0924+301	...	0.0266	...	23.52	0.4	2	<-2.64	<17.98	2
0928+678	NGC 2892	0.0225	...	22.82	30.0	12	-0.52	19.15	5
1142+198	3C 264	0.0206	0.99 ^{<i>d</i>}	24.57	200.0	1,3	-1.00	20.15	5
1205+255	UGC 7115	0.0226	...	22.58	44.0	11	-0.51	19.48	5
1216+061	3C 270	0.0074	0.46 ^{<i>d</i>}	24.31	308.0	1,3	-1.44	17.56	5
1220+587	NGC 4335	0.0154	0.41 ^{<i>d</i>}	22.64	15.0	6	-0.44	<19.01	5
1222+131	3C 272.1	0.0037	0.15 ^{<i>l</i>}	23.22	180.0	1,3	-1.18	18.17	5
1228+126	3C 274	0.0037	...	24.63	4000.0	1,3	-1.24	19.18	5
1257+282	NGC 4874	0.0239	...	23.07	1.2	2	-1.87	<17.49	2
1322+366	NGC 5141	0.0173	0.25 ^{<i>l</i>}	23.63	78.7	10	-0.61	<18.69	5
1336+391	3C 288	0.2460	...	26.42	30.0	1,3	-1.56	20.03	1
1346+268	4C 26.42	0.0633	...	24.52	59.3	2	-0.78	19.58	2
1407+177	NGC 5490	0.0162	0.35 ^{<i>l</i>}	23.24	37.8	10	-1.28	<17.48	5
1414+110	3C 296	0.0237	0.29 ^{<i>d</i>}	24.61	77.0	1,3	-1.33	18.64	1
1422+268	...	0.0370	...	23.99	21.1	2	-1.15	<19.41	2
1430+251	4C 25.46	0.0813	...	24.20	1.2	2	<-1.93	<19.61	2
1450+281	...	0.1265	...	24.48	6.7	2	-1.12	<19.77	2
1502+261	3C 310	0.0540	...	25.19	80.0	1,3	-1.19	19.38	1
1510+709	3C 314.1	0.1197	...	25.33	<1.0	1,3	<-2.55	<19.52	1
1514+072	3C 317	0.0342	...	24.43	391.0	1,3	-0.13	19.49	1
1521+288	4C 28.39	0.0825	...	24.53	55.8	2	-0.60	20.20	2
1527+308	...	0.1143	...	24.03	4.0	2	-0.97	<19.89	2
1553+245	...	0.0426	...	23.43	57.9	2	-0.03	19.84	2
1610+296	NGC 6086	0.0313	...	22.92	1.1	2	<-1.52	<18.38	2
1613+275	...	0.0647	...	24.01	10.6	2	-1.00	<19.24	2
1626+396	3C 338	0.0303	...	24.19	105.0	1,3	-0.57	19.33	1
1637+826	NGC 6251	0.024	...	23.82	720.0	13,4	0.44	20.19	7
1641+173	3C 346	0.1620	...	26.20	220.0	1,3	-0.82	21.17	1
1648+050	3C 348	0.1540	...	27.12	10.0	1,3	-3.13	19.67	1
1827+323	...	0.0659	...	24.04	20.8	2	-0.71	<19.38	2
2045+068	3C 424	0.1270	...	25.67	18.0	1,3	-1.58	<19.77	1
2116+262	NGC 7052	0.0164	0.30 ^{<i>d</i>}	22.97	47.0	9,14	-0.22	18.26	8
2153+377	3C 438	0.2900	...	26.77	17.0	1,3	-2.02	<19.94	1
2212+135	3C 442	0.0262	...	24.39	2.0	1,3	-2.61	18.16	1
2229+391	3C 449	0.0181	0.50 ^{<i>d</i>}	24.29	37.0	1,3	-1.56	19.13	1
2236+350	UGC 12127	0.0277	...	23.46	7.1	2	-1.34	18.55	2
2318+079	NGC 7626	0.0113	0.17 ^{<i>l</i>}	22.39	15.6	10	-1.47	<17.91	5
2335+267	3C 465	0.0301	0.69 ^{<i>l</i>}	25.00	270.0	1,3	-0.97	19.60	1

Superscripts ‘*d*’ and ‘*l*’ for *b/a* stand for extended dust disks and lanes, respectively. References: (1) : Chiaberge et al. (1999) (F702W filter); For the 7 sources which were common between the 3CR, B2 and the UGC samples we used the F555W flux densities from Verdoes Kleijn et al. (2002); (2) : Capetti et al. (2002) (1.4 GHz, F814W filter); (3) : Kuehr et al. (1979) (5 GHz); (4) : Kuehr et al. (1981) (5 GHz); (5) : Verdoes Kleijn et al. (2002) (F555W filter); (6) : Xu et al. (2000) (1.4 GHz); (7) : Hardcastle & Worrall (1999) (F702W filter); (8) : (Capetti & Celotti 1999) (F814W filter); (9) : Giovannini et al. (1988) (5 GHz); (10) : Bridle & Perley (1984) (core at 5 GHz, total flux density at 1.4 GHz); (11) : Laurent-Muehleisen et al. (1997) (5 GHz); (12) : Jenkins (1982) (5 GHz); (13) : Waggett et al. (1977) (2.7 GHz); (14) : Gregory & Condon (1991) (5 GHz); (15) : Becker et al. (1991) (5 GHz).

Table 2. The FRII radio galaxies.

IAU name	Alternate name	Redshift <i>z</i>	<i>b/a</i>	$\log L_{ext}$ W Hz $^{-1}$	S_c (5 GHz) mJy	ref.	$\log R_c$	$\log L_o$ W Hz $^{-1}$	ref.
0034-014	3C 15	0.073	...	25.46	372.8	1,3	-0.52	<19.74	1
0035-024	3C 17*	0.220	...	26.63	727.9	1,3	-0.48	21.64	1
0038+097	3C 18	0.188	...	26.41	118.2	1,3	-1.18	21.36	1
0106+729	3C 33.1*	0.181	...	26.11	19.7	1,3	-1.69	20.94	1
0109+492	3C 35	0.067	...	25.06	23.7	1,3	-1.40	<19.31	1
0218-021	3C 63	0.175	...	26.10	18.3	1,3	-1.74	21.04	1
0307+169	3C 79	0.256	...	26.62	14.7	1,3	-2.03	21.02	1
0325+023	3C 88	0.030	...	24.86	197.2	1,3	-0.97	19.46	1
0356+102	3C 98	0.030	...	25.25	11.1	1,3	-2.61	<18.53	1
0415+379	3C 111*	0.049	...	25.86	1155.3	1,4	-0.77	20.99	1
0433+295	3C 123	0.218	...	27.55	85.0	1,3	-2.33	<19.16	1
0453+227	3C 132	0.214	...	26.35	33.5	1,3	-1.56	<19.55	1
0459+252	3C 133	0.277	...	26.85	170.8	1,3	-1.14	20.68	1
0511+008	3C 135	0.127	...	25.88	5.5	1,3	-2.31	20.15	1
0605+480	3C 153	0.277	...	26.68	0.4	1,3	-3.56	<19.34	1
0640+233	3C 165	0.296	...	26.48	8.7	1,3	-2.01	19.95	1
0642+214	3C 166	0.245	...	26.15	553.6	1,3	-0.03	20.71	1
0651+542	3C 171	0.238	...	26.49	2.5	1,3	-2.74	19.20	1
0734+805	3C 184.1	0.118	...	25.87	7.5	1,3	-2.23	20.96	1
0802+243	3C 192	0.060	...	25.56	8.5	1,3	-2.44	<19.94	1
0818+472	3C 197.1	0.131	...	25.82	6.8	1,3	-2.13	20.88	1
0819+061	3C 198	0.082	...	25.14	<1.5	5,4	<-2.50	20.85	1
0917+458	3C 219*	0.174	...	26.49	68.7	1,3	-1.56	21.39	1
0936+361	3C 223	0.137	...	26.04	11.7	1,3	-2.07	<20.05	1
0938+399	3C 223.1	0.108	...	25.65	8.7	1,3	-2.02	<19.98	1
0945+076	3C 227*	0.086	...	25.94	23.5	1,3	-2.07	21.66	1
0958+290	3C 234*	0.185	...	26.34	133.6	1,3	-1.07	21.85	1
1003+351	3C 236	0.099	...	25.70	191.5	1,3	-0.80	<19.84	1
1205+341	...	0.0788	...	24.46	12.5	2	-1.21	<19.81	2
1251+278	3C 277.3	0.0857	...	25.37	12.4	2	-2.05	19.49	2
1319+428	3C 285	0.079	...	25.32	7.8	1,3	-2.00	18.47	1
1330+022	3C 287.1*	0.216	...	26.34	443.8	1,3	-0.42	21.43	1
1420+198	3C 300	0.270	...	26.58	10.1	1,3	-2.12	20.47	1
1441+522	3C 303*	0.141	...	25.83	187.6	1,3	-0.64	21.44	1
1519+078	3C 318.1	0.046	...	24.49	3.0	6,3	-2.05	<18.52	1
1522+546	3C 319	0.192	...	26.04	1.4	1,3	-2.72	<20.14	1
1545+210	3C 323.1*	0.264	...	26.44	43.8	1,3	-1.36	22.83	1
1549+202	3C 326	0.089	0.24 ^d	25.19	15.9	1,3	-1.46	<19.91	1
1559+021	3C 327	0.104	...	26.18	40.8	1,3	-1.91	<19.35	1
1615+325	3C 332*	0.152	...	25.93	11.5	1,3	-1.89	21.56	1
1658+471	3C 349	0.205	...	26.33	21.9	1,3	-1.76	20.88	1
1717-009	3C 353	0.030	...	25.94	216.2	1,3	-2.01	<18.40	1
1726+318	3C 357	0.167	...	26.10	6.5	1,3	-2.23	<19.66	1
1825+743	3C 379.1	0.256	...	26.32	3.9	7,3	-2.32	<19.91	1
1832+474	3C 381	0.161	...	26.18	6.9	1,3	-2.31	<20.28	1
1833+326	3C 382*	0.058	...	25.47	228.1	1,4	-0.95	22.56	1
1842+455	3C 388	0.091	...	25.80	76.5	1,3	-1.37	20.07	1
1845+797	3C 390.3*	0.056	...	25.74	434.7	1,3	-0.97	21.88	1
1939+605	3C 401	0.201	...	26.41	47.5	1,3	-1.52	20.35	1
1940+505	3C 402	0.025	...	24.39	48.1	1,3	-1.27	19.46	1
1949+023	3C 403	0.059	...	25.54	12.1	1,3	-2.28	19.49	1
2221-023	3C 445*	0.057	...	25.40	382.8	1,3	-0.66	22.11	1
2243+394	3C 452	0.081	0.27 ^l	25.96	152.3	1,3	-1.33	<19.72	1
2309+090	3C 456	0.233	...	26.24	27.8	1,3	-1.45	21.21	1
2318+235	3C 460	0.268	...	26.02	21.4	1,4	-1.24	20.29	1

Superscripts ‘*d*’ and ‘*l*’ for *b/a* stand for extended dust disks and lanes, respectively. There are only two FRIIs for which *b/a* for extended dust features are available (de Koff et al. 2000). We do not include the FRIIs in our analysis of the extended dusty disks. Sources with a star are BLRGs. References : (1) : Chiaberge et al. (2002) (5 GHz, F702W filter, except 3C 192 observed with F555W); (2) : Capetti et al. (2002) (1.4 GHz); (3) : Kuehr et al. (1979) (5 GHz); (4) : Veron-Cetty & Veron (1998) (5 GHz); (5) : Fomalont & Bridle (1978) (5 GHz); (6) : Sree et al. (1989) (1.5 GHz); (7) : Spangler & Sakurai (1985) (1.4 GHz).

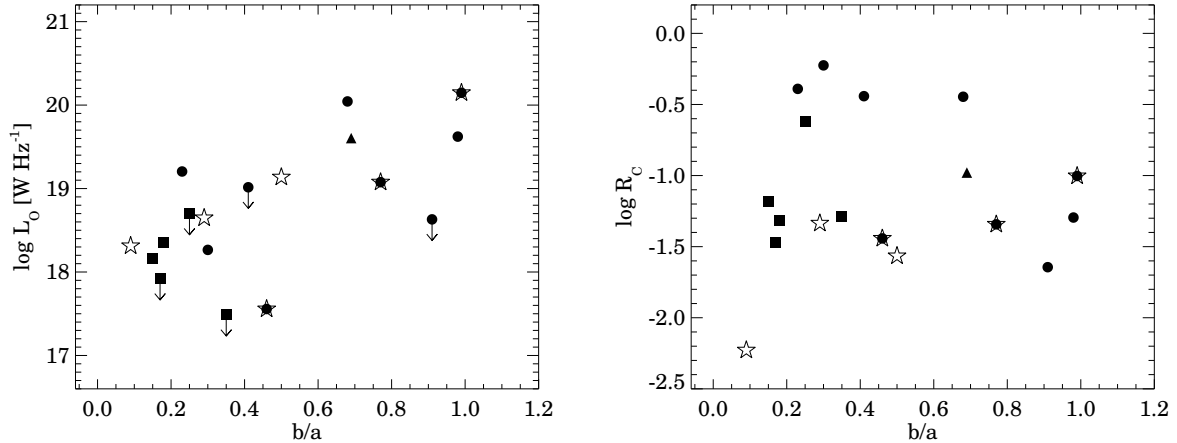


Fig. 2. Nuclear optical luminosity L_o (left) and radio core prominence R_c (right) plotted against b/a for the FRI radio galaxies. The \bullet and \blacksquare denote the dust disks and lanes respectively, from Verdoes Kleijn et al. (1999) while the open star and \blacktriangle denote the dust disks and lanes from de Koff et al. (2000), \downarrow denote upper limits. The sources common to both the papers are shown by an open star superimposed by a \bullet . Table 5 lists the statistics for the correlations.

3. Comparison with the optical nuclei of the beamed objects and the Unified Scheme

In the simple Unified Scheme, the beamed counterparts of the FRI and FRII radio galaxies are the BL Lac objects and the radio-loud quasars respectively. In §2.1 we find the optical emission from galaxy cores to be orientation-dependent. Given that optical emission from BL Lacs and quasars is also beamed (e.g., Kapahi & Shastri 1987; Baker et al. 1994), we attempt to relate the galaxy behaviour to that of BL Lacs and quasars in the framework of the Unified Scheme. We use this framework to extend the correlations of nuclear optical luminosity with radio core prominence to higher values of radio core prominence. We consider the FRI radio galaxies and BL Lacs together and henceforth refer to them as the “FRI population”, and similarly consider the FRII radio galaxies and radio-loud quasars together and henceforth refer to them as the “FRII population”. In order to investigate quantitatively the dependence of the optical emission on orientation, we come up with a model-fitting approach. We attempt to apply this to the available data and present the results in §3.5.3. We further outline the caveats and the drawbacks of our current sample and attempt to address them in §3.4.

3.1. The data

We have considered BL Lac objects which are both X-ray selected (belonging to *EMSS* and *HEAO-1* samples) and radio-selected, from Perlman & Stocke (1993); Vermeulen & Cohen (1994) and Laurent-Muehleisen et al. (1993). We have thus attempted to include both the high R_c (Vermeulen & Cohen 1994) and intermediate R_c (Laurent-Muehleisen et al. 1993) BL Lacs. The BL Lacs which showed FRII radio morphology in the form of terminal hotspots *viz.*, 1308+326, 1823+568, 2007+777 (Kollgaard et al. 1992), 1749+701 (O’Dea et al. 1988) and 1803+784 (Cassaro et al. 1999); which were gravitational microlensing candidates, *viz.*, 1413+135 (this object also has other peculiarities like a spiral host galaxy; Perlman & Stocke 1993) and which had uncertain redshifts *viz.*, 0716+714, were excluded from our set of BL Lacs. Our BL Lac sample finally has 44 objects spanning a redshift range of $0.028 \leq z \leq 0.997$. For the beamed counterparts of FRII radio galaxies, we considered 34 high R_c radio-loud quasars from Vermeulen & Cohen (1994) spanning the redshift range of $0.158 \leq z \leq 2.367$.

We have taken the total optical luminosity of BL Lacs and quasars (as derived from their available V-band magnitudes) as the optical core luminosity, *assuming that the core overwhelms the host galaxy emission*. As the BL Lacs are known to be strongly variable, we took radio and optical measurements from the literature that were as closely spaced in time as was available. Several V-magnitudes come from optical monitoring campaigns of Pica et al. (1988); Webb et al. (1988) and Falomo et al. (1994). Quasars also can be Optically Violent Variables (OVVs) but OVVVs constitute less than 25% of the quasars used in our analysis. The data are tabulated in Tables 3 and 4. Col. (1) lists the IAU name (B1950); Col. (2) Alternate name; Col. (3) Redshift (from the references for radio core data, except 1402+042, 0333+321, 0835+580 and 0836+710 which are from Veron-Cetty & Veron (1998)); Col. (4) V-band magnitude; Col. (5) reference for m_v ; Col. (6) logarithm of extended radio luminosity at 1.4 GHz in W Hz^{-1} – taken from the reference for radio core flux density for BL Lacs and calculated using core flux density and radio core prominence for quasars

Table 3. The BL Lac objects.

IAU name	Alternate name	Redshift z	m_v	ref.	$\log L_{ext}$ W Hz $^{-1}$	S_c (5 GHz) mJy	ref.	$\log R_c$	$\log L_o$ W Hz $^{-1}$
0158+003	...	0.299	17.96	1	24.36	8.38	2	0.60	22.61
0219-164	...	0.698	17.0	9	25.50	358.0	5	0.84	23.78
0219+428	3C 66A	0.444	15.08	6	27.32	814.0	2 ^a	0.14	24.13
0257+344	...	0.247	18.53	1	23.22	11.78	2	1.69	22.21
0317+185	...	0.190	18.12	1	23.50	9.85	2	1.08	22.13
0323+022	...	0.147	16.98	6	23.20	55.0	5	1.21	22.36
0414+009	...	0.287	17.11	6	24.50	67.0	5	0.54	22.91
0454+844	...	1.34*	17.3	9	24.21	1400.0	4	>3.37 [†]	24.29
0521-365	...	0.055	14.62	9	26.12	3124.0	2 ^a	-0.14	22.43
0548-322	...	0.069	16.05	8	24.67	80.0	2 ^a	-0.08	22.06
0607+711	...	0.267	19.60	1	24.79	14.08	2	0.29	21.85
0706+592	...	0.124	18.40	9	24.20	65.0	5	0.17	21.64
0735+178	...	>0.424	15.40	9	23.82	1990.0	4	>3.2	23.96
0737+746	...	0.315	16.89	1	23.85	24.47	2	1.64	23.09
0851+202	OJ287	0.306	13.81	7	24.21	2217.0	2 ^a	3.23	24.29
1101-232	...	0.186	17.01	8	24.40	49.0	5	0.41	22.56
1101+384	Mrk421	0.030	13.22	6	23.85	520.0	2 ^a	0.81	22.46
1133+704	Mrk180	0.044	14.49	9	24.31	131.0	2 ^a	0.09	22.29
1218+304	...	0.130	15.80	6	22.79	62.0	5	>1.34	22.72
1219+285	ON 231	0.102	15.40	7	23.07	2058.0	2 ^a	3.25	22.67
1221+248	...	0.218	17.65	1	23.64	27.85	2	1.53	22.45
1229+645	...	0.164	16.89	1	23.73	42.49	2	1.34	22.49
1235+632	...	0.297	18.59	1	24.00	13.0	5	>0.32	22.35
1400+162	...	0.244	16.74	9	26.27	233.0	2 ^a	-0.07	22.91
1402+042	...	0.344	16.88	8	24.40	21.43	2	0.53	23.17
1407+599	...	0.495	19.67	1	25.76	14.12	2	0.08	22.39
1418+546	...	0.152	15.39	6	24.31	1058.0	2 ^a	2.09	23.03
1426+427	...	0.130	16.40	9	23.50	31.0	5	>1.04	22.48
1443+638	...	0.299	19.65	1	24.63	8.36	2	0.33	21.93
1458+228	...	0.235	16.79	1	23.98	29.0	2	1.28	22.86
1514-241	AP Lib	0.049	14.97	7	23.61	2562.0	2 ^a	2.18	22.19
1534+018	...	0.312	18.70	1	25.28	28.84	2	0.26	22.35
1538+149	4C 14.60	0.605	17.89	6	26.94	1337.0	2 ^a	1.17	23.29
1552+203	...	0.222	17.70	1	24.65	33.09	2	0.61	22.44
1652+398	Mrk501	0.034	14.08	6	23.52	1376.0	2 ^a	1.66	22.23
1727+502	...	0.055	16.12	6	23.83	175.0	2 ^a	0.89	21.83
1749+096	...	0.320	17.32	6	23.89	744.0	2 ^a	>3.11	22.93
1807+698	3C 371	0.050	14.57	7	25.04	1350.0	2 ^a	0.48	22.37
2143+070	...	0.237	18.04	1	24.99	44.63	2	0.46	22.37
2155-304	...	0.117	13.31	6	25.18	252.00	2 ^a	0.37	23.62
2200+420	BL Lac	0.069	15.42	7	23.93	3310.00	2 ^a	2.26	22.31
2201+044	...	0.028	15.47	8	23.70	316.00	5	0.25	21.50
2254+074	...	0.190	16.29	6	24.51	454.00	2 ^a	1.73	22.87
2356-309	...	0.165	17.18	8	23.50	42.00	5	0.90	22.38

Redshift with a star is from Rector & Stocke (2001) – $\log R_c$ [†] was thus calculated for this new z using the $\log R_c$ quoted in Vermeulen & Cohen (1994). References : (1) : Morris et al. (1991); (2) : Perlman & Stocke (1993) (EMSS XBLs except 2^a which are RBLs, 1.4 GHz); (4) : $\log R_c$ from Vermeulen & Cohen (1994); (5) : Laurent-Muehleisen et al. (1993) (HEAO-1 XBLs, 1.5 GHz); (6) : Pica et al. (1988); (7) : Webb et al. (1988); (8) : Falomo et al. (1994); (9) : Padovani & Giommi (1995).

and the BL Lacs 0454+844 and 0735+178; data at 5 GHz converted to 1.4 GHz using $\alpha_{radio}^{ext} = 0.7$ for extended radio emission; Col. (7) 5 GHz radio core flux density in mJy; Col. (8) reference for the radio core and total flux density (for quasars it is the reference for the radio core flux density and $\log R_c$); Col. (9) logarithm of radio core prominence standardized to an emitted wavelength of 6 cm; Col. (10) optical core luminosity in W Hz $^{-1}$ estimated at an emitted wavelength of 5500 Å. The plots of nuclear optical luminosity against radio core prominence parameter are shown in Fig. 3.

Table 4. The Radio-loud quasars.

IAU name	Alternate name	Redshift z	m_v	ref.	$\log L_{ext}$ W Hz $^{-1}$	S_c (5 GHz) mJy	ref.	$\log R_c$	$\log L_o$ W Hz $^{-1}$
0016+731	...	1.781	19.00	4	27.37	>1500.0	1	>0.7	23.88
0106+013	...	2.107	18.39	4	27.65	3470.0	1	0.9	24.29
0153+744	...	2.338	16.00	4	26.26	1510.0	1	>2.0	25.35
0212+735	...	2.367	20.00	4	25.03	2200.0	1	>3.4	23.76
0234+285	...	1.207	18.50	4	25.68	1440.0	1	2.1	23.71
0333+321	NRAO140	1.259	17.50	4	26.44	2460.0	1	1.6	24.15
0458-020	...	2.286	19.50	4	27.17	1600.0	1	1.1	23.93
0615+820	...	0.710	17.50	4	26.38	>900.0	1	>0.8	23.60
0711+356	...	1.620	19.00	4	25.96	1500.0	1	>2.1	23.79
0723+679	3C 179	0.846	18.00	4	27.54	320.0	1	-0.68	23.57
0835+580	3C 205	1.536	17.62	4	27.89	23.0	1	-1.74	24.29
0836+710	...	2.180	16.50	4	27.04	2550.0	1	1.4	25.08
0839+616	...	0.862	17.85	4	26.84	34.0	1	-0.94	23.64
0850+581	...	1.322	18.00	4	27.45	1090.0	1	0.27	23.99
0906+430	3C 216	0.670	18.10	4	27.21	1060.0	1	-0.01	23.30
0923+392	4C 39.25	0.698	17.86	4	26.77	7320.0	1	1.3	23.44
1039+811	...	1.260	16.50	4	26.20	1120.0	1	1.5	24.55
1040+123	3C 245	1.028	17.29	4	27.44	860.0	1	0.0	24.04
1150+812	...	1.250	18.50	4	26.50	1140.0	1	1.2	23.74
1156+295	...	0.729	14.41	4	26.32	810.0	1	0.83	24.86
1222+216	4C 21.35	0.435	17.50	4	26.47	420.0	1	-0.01	23.14
1226+023	3C 273	0.158	12.85	4	26.70	39000.0	1	0.9	24.08
1253-055	3C 279	0.538	17.75	4	27.07	14500.0	1	1.1	23.24
1458+718	3C 309.1	0.905	16.78	4	27.63	2680.0	1	0.2	24.12
1641+399	3C 345	0.594	15.96	4	26.33	5520.0	1	1.5	24.05
1642+690	...	0.751	20.50	4	26.67	1260.0	1	0.7	22.45
1721+343	4C 34.47	0.206	15.46	4	25.95	470.0	1	-0.05	23.27
1828+487	3C 380	0.691	16.81	4	27.32	6590.0	1	0.7	23.85
1830+285	4C 28.45	0.594	17.16	4	27.02	450.0	1	-0.28	23.57
1901+319	3C 395	0.635	17.50	4	26.81	1480.0	1	0.5	23.49
1928+738	...	0.302	16.06	4	25.75	3210.0	1	1.3	23.38
1951+498	...	0.466	17.50	4	26.09	91.0	1	-0.24	23.20
2223-052	3C 446	1.404	18.39	4	28.24	2310.0	1	-0.15	23.90
2251+158	3C 454.3	0.859	16.10	4	27.05	9690.0	1	1.3	24.34

References : (1) : $\log R_c$ from Vermeulen & Cohen (1994); (4) : Veron-Cetty & Veron (1998).

3.2. Caveats

While interpreting the $L_o - R_c$ plots, it is important to keep the following caveats in mind.

1. The objects constitute an *eclectic* sample, with no rigorous selection criteria applied.
2. The beamed and unbeamed objects are not matched in redshift, nor in extended radio luminosity. We discuss the significance of this in §3.3 and try to come up with a ‘matched’ sample in §3.4.
3. The L_o values for the BL Lacs and quasars are derived from their total magnitudes, and include the host galaxy contribution. Particularly in the intermediate R_c regime for BL Lacs, the host galaxies could contribute significantly to the assumed nuclear optical luminosity.

We address some of these issues later in the paper.

3.3. Correlations with radio core prominence for the two populations

For both the FR populations, the correlation *does* extend to higher radio core prominence, broadly consistent with the predictions of the Unified Scheme and again reinforcing the idea that the nuclear optical flux density is orientation-dependent in the same way as the core radio emission and it may thus constitute the optical counterpart of the relativistically beamed radio synchrotron jet. Using survival analysis, the generalized Spearman’s Rank correlation test indicates that the FRI and FRII populations both show a significant correlation ($p < 0.0001$) of nuclear optical luminosity with radio core prominence (see Table 5).

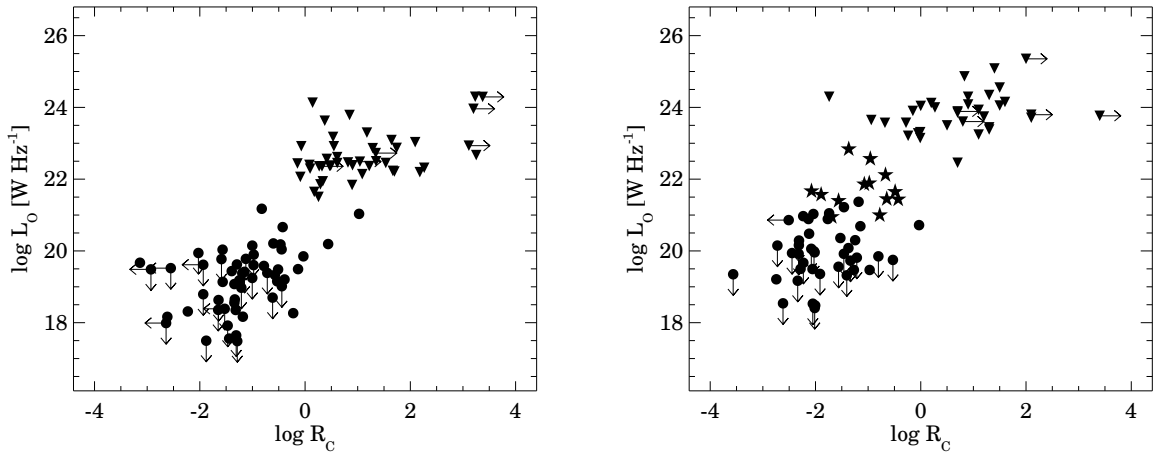


Fig. 3. Nuclear optical luminosity L_o versus radio core prominence R_c for the FRI population (left) : • denote radio galaxies, ▼ denote BL Lac objects. L_o vs. R_c for the FRII population (right) : • denote radio galaxies, ▼ are radio-loud quasars and ★ are BLRGs. ↓ and ← denote upper limits, → denote lower limits. Statistics for the fits are listed in Table 5.

For the FRII population, we showed in §2.1 that the narrow-line FRIIs do not show any correlation by themselves. A significant correlation ($p < 0.0001$, generalized Spearman Rank test) exists for the broad-line objects, however, *i.e.*, the broad-line radio galaxies and quasars. These two observations taken together are consistent with there being obscuration effects by a torus in the FRIIs. Also, though more FRIs show detected optical cores as compared to FRIIs, optical cores have been detected in *all* the BLRGs observed (where the US predicts no obscuration by the torus), again consistent with this idea.

The BL Lacs by themselves also show a significant correlation of L_o with R_c , but the plot is flatter than what is expected from beaming alone. This could be due to the fact that their L_o values include the contribution from the host galaxy, particularly since this contamination is likely to be more severe at intermediate values of R_c . Although for many BL Lac objects where host galaxies have been imaged, the difference between the nuclear and the total optical luminosity (L_o) is less than the 50% errors assumed in L_o (for e.g., Jannuzi et al. 1997), for some sources this difference can as high as a magnitude (e.g., Kotilainen et al. 1998). In principle, the flattening could also be due to the presence of a luminous accretion disk, in which case the BL Lacs cannot be considered to be consistent with the unbeamed FRI radio galaxies. The use of nuclear luminosities uncontaminated by host galaxy emission for *all* the objects would clarify the issue. We are in the process of investigating this point which is part of a future paper.

A two-dimensional Kolmogorov-Smirnov test shows that the FRI and FRII populations are different at the $p < 0.0001$ level. For each of the populations, a multiple linear regression test using the statistics packages STATISTICA and ASURV (the ‘Buckley James’ algorithm) with radio core prominence, redshift and extended radio luminosity (L_{ext}) as independent variables for the nuclear optical luminosity, shows that the correlation coefficient for the $L_o - R_c$ correlation is the most significant ($p < 0.0001$). Extended radio luminosity is the next most significant contributor. Since the extended radio luminosity can reasonably be assumed to be an indicator of intrinsic AGN power, this implies that variation in intrinsic nuclear power contributes significantly to the scatter in the $L_o - R_c$ correlation. As expected, the nuclear optical luminosity is correlated with redshift, both because luminosity is expected to correlate with redshift, and because of the absence of high redshift radio galaxies in the samples.

3.4. Matched subsamples of FRI and FRII objects

Ideally, all the objects in each population ought to be intrinsically similar in the framework of the Unified Scheme, which means that they should all be of similar intrinsic power, from the same volume of space, and with a narrow distribution of other orientation-independent parameters. As a next best step, we attempt here to derive a ‘matched’ sample for the two FR populations, keeping in mind the multiple linear regression results for the whole sample discussed in the previous section.

For the FRI matched subsample, we restrict the redshifts to $z < 0.3$ and extended radio luminosity at 1.4 GHz to be $23.5 \leq \log L_{ext} \leq 25$ W Hz⁻¹. For the FRII matched subsample, the redshifts are constrained to $z < 1.3$, while the extended radio luminosity is $26.2 \leq \log L_{ext} \leq 27.6$ W Hz⁻¹. Figure 4 shows the $L_o - R_c$ correlations for these subsamples while the correlation and regression parameters are listed in Table 5. We find that the scatter seen in Fig. 3

is considerably reduced in Fig. 4 and the correlations improve significantly compared to the unrestricted samples. Multiple linear regression tests on the restricted samples with the independent variables, R_c , z , L_{ext} show that the $L_o - R_c$ is still the strongest correlation ($p < 0.0001$) while the contribution of L_{ext} is no longer significant.

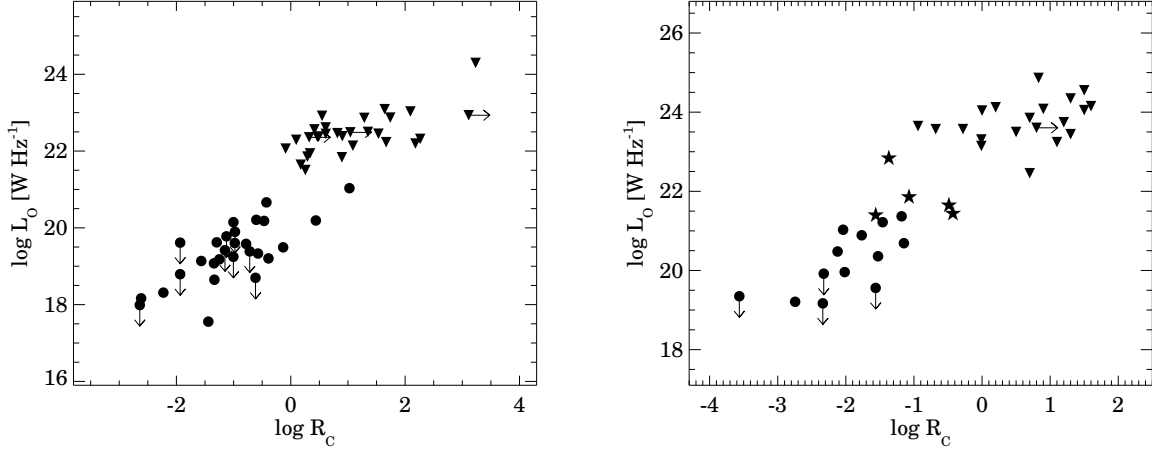


Fig. 4. Nuclear optical luminosity L_o versus radio core prominence R_c for the matched subsample of FRI galaxies and BL Lac objects (left) and FRII galaxies and quasars (right). • denote radio galaxies, ▼ denote BL Lac objects (left) and quasars (right), ★ are BLRGs, ↓ denote upper limits while → denote lower limits. Statistics for the fits are listed in Table 5.

3.5. Model-fitting the $L_o - R_c$ data

If bulk relativistic motion with a single Lorentz factor (γ) value applicable to the whole population were alone responsible for the variation in the nuclear optical luminosity, then the logarithmic plot of L_o against R_c would be linear. Any additional factors such as orientation effects due to a torus or thin thermal disk will cause this relationship to deviate from linearity. We attempt to fit some simple models to the data along these lines.

3.5.1. The model equations and the bulk Lorentz factor

We assume that the nuclear optical luminosity L_o is, in the most general case, due to the sum of synchrotron emission from the base of a relativistic jet, and thermal emission from a thin accretion disk, modified by the presence of an optically thick torus. Keeping in mind, however, that we are only attempting to explore the potential of such a model-fitting approach and that our sample is not rigorously selected, we consider a very simple model here. We do not include the possibility of variation in the *intrinsic* nuclear power as discussed in §3.3, nor the possibility of extinction of the optical nucleus by an extended kpc-scale dusty disk which was discussed in §2.2. Our models also do not take into account any intrinsic spread in the Lorentz factors, nor the possibility that the relevant Lorentz factor for the highly beamed and mildly beamed subclasses may be systematically different due to a “spine-sheath” type structure of the jet (e.g., Hardcastle et al. 1996; Laing et al. 1999). However, as the multiple linear regression tests discussed in §3.3 suggest, orientation appears to play the most dominant role in the variation of L_o . We write,

$$L_o = (\delta^p L_{jet}^{int} + L_{disk} \cos \theta) \times 10^{-A_V/2.5} \quad (1)$$

L_{jet}^{int} is the intrinsic synchrotron luminosity from the base of the jet which is relativistically beamed by the factor δ^p , where δ is the Doppler factor and for a jet spectral index of α , the jet structure parameter p is given by $2+\alpha$ or $3+\alpha$ depending on whether the jet is continuous or blobby (e.g., Urry & Padovani 1995). L_{disk} is the luminosity of a thin optically thick accretion disk, whose apparent luminosity is orientation-dependent due to projection (the $\cos \theta$ term). A_V is the extinction resulting from the torus in the V band. For a half-opening angle of the torus θ_c , we have,

$$A_V = A_{V_0} \left(1 - \frac{\cos \theta}{\cos \theta_c} \right) \quad \text{for} \quad \theta \geq \theta_c \quad (2)$$

Table 5. Statistics of correlations.

Type	N (l_x, l_y)	X	Y	Spearman	Kendall	Schmitt(slope, intercept)
FRI galaxies	54 (5,17)	$\log R_c$	$\log L_o$	0.0001	0.0001	0.52(0.17) 19.40(0.25)
BL Lacs	44 (6,0)	$\log R_c$	$\log L_o$	0.0295	0.0323	0.17(0.14) 22.45(0.16)
FRI & BL Lacs	98 (11,17)	$\log R_c$	$\log L_o$	<0.0001	<0.0001	1.15(0.10) 20.72(0.14)
FRI-BL sample	57 (1,2)	$\log R_c$	$\log L_o$	<0.0001	<0.0001	1.20(0.17) 20.72(0.16)
FRII galaxies	42 (1,20)	$\log R_c$	$\log L_o$	0.2175	0.2392	0.32(0.23) 20.12(0.38)
BLRGs & QSRs	47 (5,0)	$\log R_c$	$\log L_o$	<0.0001	<0.0001	0.60(0.12) 23.15(0.12)
FRII & QSRs	89 (6,20)	$\log R_c$	$\log L_o$	<0.0001	<0.0001	1.18(0.11) 22.26(0.17)
FRII-QS sample	38 (0,3)	$\log R_c$	$\log L_o$	<0.0001	<0.0001	1.12(0.11) 22.71(0.15)
FRI galaxies ^V	9 (0,2)	$b/a (d)$	$\log L_o$	0.2499 ^a	0.2310	1.83(1.22) 17.67(0.89)
"	14 (0,5)	$b/a (d + l)$	$\log L_o$	0.0928 ^a	0.0399	1.91(0.61) 17.54(0.37)
"	9 (0,0)	$b/a (d)$	$\log R_c$	0.0732 ^a	0.0953	-1.09(0.47) -0.19(0.37)
"	14 (0,0)	$b/a (d + l)$	$\log R_c$	0.6065 ^a	0.5200	-0.37(0.40) -0.80(0.23)
FRI galaxies ^D	6 (0,0)	$b/a (d)$	$\log L_o$	0.0845 ^a	0.0909	2.24(0.82) 17.62(0.48)
"	7 (0,0)	$b/a (d + l)$	$\log L_o$	0.0543 ^a	0.0509	2.33(0.76) 17.63(0.54)
"	7* (0,0)	$b/a (d)$	$\log R_c$	0.0802 ^a	0.0985	1.39(0.53) -2.30(0.29)
"	8* (0,0)	$b/a (d + l)$	$\log R_c$	0.0588 ^a	0.0833	1.51(0.48) -2.30(0.29)
FRI galaxies ^{V+D}	12 (0,2)	$b/a (d)$	$\log L_o$	0.1855 ^a	0.1531	1.53(0.70) 17.95(0.44)
"	18 (0,5)	$b/a (d + l)$	$\log L_o$	0.0353 ^a	0.0248	1.90(0.60) 17.66(0.33)
"	12 (0,0)	$b/a (d)$	$\log R_c$	0.7630 ^a	0.6808	-0.06(0.69) -1.06(0.49)
"	18 (0,0)	$b/a (d + l)$	$\log R_c$	0.9085 ^a	0.9698	0.02(0.48) -1.12(0.28)

Statistical significance of various correlations (of X and Y) and linear regression fits. All the results are derived using ASURV as implemented in IRAF. Col. (1): the subclass of objects under consideration, 'FRII galaxies' refer to narrow-line FRIIs alone, 'QSRs' refer to quasars, 'FRI-BL' and 'FRII-QS samples' refer to the matched subsamples of FRIIs and FRIIs as described in §3.4. FRI galaxies with superscripts V , D , $V + D$ refer to FRI sources from Verdoes Kleijn et al. (1999), de Koff et al. (2000) and from both papers, respectively; \star an additional FRI source – 3C 430 with a disk of $b/a = 0.15$ and $\log R_c = -2.5$ was included in the $b/a - \log R_c$ correlation; Col. (2): the number of data points and those with limits in X and Y respectively, in parenthesis; Col. (3) & (4): the independent and dependent variable respectively; b/a being the ratio of the minor-to-major axis of the extended dust feature seen in the *HST* images of radio galaxies, ' d ' and ' l ' standing for a dust disk and a lane respectively, ' $d + l$ ' refers to our jointly considering disks and lanes in the correlations; Col. (5) & (6): probability that no correlation exists between X and Y from Spearman's ρ and Kendall's τ correlation tests respectively; 'a' - Spearman Rank test is not accurate as no. of objects, $N < 30$; Col. (7): slope and intercept with standard deviation in parentheses from Schmitt's linear regression test, bootstrap approximation using 200 iterations, X bins = 10, Y bins = 10.

$$A_V = 0 \quad \text{for} \quad \theta < \theta_c \\ (\text{Simpson 1996})$$

Thus for $\theta = 90^\circ$, $A_V = A_{V_0}$. For the Lorentz factor of bulk relativistic motion of the nuclear jet we have,

$$\gamma = \left(\frac{1}{2^{p-1}} \frac{R_c^{max}}{R_c^{min}} \right)^{\frac{1}{2p}}, \quad (3)$$

$$R_c^{int} = \frac{\gamma^p R_c^{min}}{2} \quad (4)$$

where R_c^{min} and R_c^{max} are the minimum and maximum values of R_c , i.e., the values of R_c at edge-on ($\theta \sim 90^\circ$) and pole-on ($\theta \sim 0^\circ$) inclinations of the AGN respectively, and R_c^{int} is the intrinsic flux density ratio of the core and extended radio emission. We now obtain the orientation to the line of sight, θ , in terms of the core prominence, R_c . We use the relativistic beaming formulae which take into account contributions from both the approaching and receding jet (e.g., Appendix C, Urry & Padovani (1995)).

$$R_c = R_c^{int} \left[\frac{1}{[\gamma(1 - \beta \cos \theta)]^p} + \frac{1}{[\gamma(1 + \beta \cos \theta)]^p} \right] \quad (5)$$

We assume a value of 3 for the jet structure factor p . We note that Urry & Padovani (1995) infer a p value of ≈ 3 based on the observations of superluminal motion within our own galaxy by Mirabel & Rodriguez (1994). We get,

$$\beta \cos \theta = \sqrt{1 - \frac{(2b)^{2/3}}{\sqrt{R_c}(-2\sqrt{R_c} + \sqrt{2b + 4R_c})^{1/3}} + \frac{(2b)^{1/3}(-2\sqrt{R_c} + \sqrt{2b + 4R_c})^{1/3}}{\sqrt{R_c}}} \quad (6)$$

where $b = \frac{R_c^{int}}{\gamma^p}$.

As an approximation we assume that a single γ value is applicable to each population, and that all orientations are represented in each population, and therefore that the minimum and maximum values of R_c in each population, correspond to orientations perpendicular and parallel to our line of sight respectively. The formula using the R_c^{min} and R_c^{max} (Eq. 3) resulted in the lower limit to the maximum Lorentz factor $\gamma_{max} \approx 9.7$ for the FRI population. For the FRII population we get a value of $\gamma_{max} \gtrsim 11.5$, obtained using a quasar with a upper limit to its extended radio emission, and therefore the actual lower limit to γ_{max} could be higher. These values broadly agree with those obtained by Urry & Padovani (1995) : $\gamma_{max} \gtrsim 9$ for the FRI population and $\gtrsim 13$ for the FRII population assuming $p = 3$. However, based on the correlation of optical and radio core emission with the isotropic H α +[NII] emission Verdoes Kleijn et al. (2002) have obtained a constraint on the value of γ of $\lesssim 2$ (assuming $p = 3$), albeit for FRI radio galaxies *alone*.

3.5.2. The models and the fitting procedure

We considered several simple models to compare the behaviour of the optical nuclei in the FRI and FRII populations. For the ‘Jet-only’ model, the entire nuclear optical luminosity is ascribed to synchrotron emission from a jet which is relativistically beamed. For the ‘Jet+Disk’ model, the nuclear optical luminosity is modelled as a combination of a beamed synchrotron jet and a thin optically thick disk. For the ‘Jet+Disk+Torus’ model, Eq. 1 is used *in toto*. In the ‘Jet+Torus’ model the entire nuclear optical luminosity is due to the beamed jet, modified by an obscuring torus.

Table 6. Parameters from the different model-fits for the FR populations.

	Model	A_{V_0}	θ_c	Model		Outputs		
				L_{jet}^{int}	σ	L_{disk}	σ	AIC
FRI	Jet only	2.7e+20	1.3e+19	295.2
	Jet+Disk	2.6e+20	1.4e+19	8.5e+17	1.1e+18	297.1
	Jet+Disk+Torus	3.0	45	2.7e+20	1.5e+19	3.5e+18	1.6e+18	304.5
	Jet+Torus	3.0	45	2.9e+20	1.4e+19	303.1
	Best fit	0.1	90	2.6e+20	1.3e+19	295.3
Matched FRI	Jet only	3.8e+20	2.5e+19	132.3
	Jet+Disk	4.1e+20	2.9e+19	-7.9e+18	2.0e+18	133.4
	Jet+Disk+Torus	3.0	45	4.4e+20	3.3e+19	-1.4e+18	4.1e+18	137.0
	Jet+Torus	3.0	45	4.4e+20	2.9e+19	135.0
FRII	Jet only	5.8e+21	3.0e+20	269.6
	Jet+Disk	6.5e+21	3.7e+20	-6.7e+19	1.2e+19	270.7
	Jet+Disk+Torus	3.0	45	6.7e+21	3.9e+20	-5.8e+19	1.5e+19	272.9
	Jet+Torus	3.0	45	6.1e+21	3.2e+20	271.5
	Best fit	3.0	37	6.5e+21	3.4e+20	270.8
Matched FRII	Jet only	1.6e+21	1.3e+20	94.3
	Jet+Disk	1.8e+21	1.5e+20	-1.9e+20	2.1e+19	93.4
	Jet+Disk+Torus	3.0	45	2.0e+21	1.7e+20	-2.1e+20	2.5e+19	95.9
	Jet+Torus	3.0	45	1.8e+21	1.4e+20	96.2
BL FRII	Jet only	2.2e+22	1.6e+21	127.3
	Jet+Disk	1.3e+22	1.2e+21	1.5e+22	2.7e+21	123.3
BL Lacs*	Jet only	1.2e+21	9.0e+19	118.4
	Jet+Disk	6.2e+19	1.4e+19	3.3e+22	3.0e+21	78.6

* See §3.5.3 in the text. In Col.(1) FRI/FRII and Matched FRI/FRII stand for the FRI/FRII population and it’s matched subsample as discussed in §3.4, BL FRII stand for the broad-line FRIIs *viz.*, BLRGs and quasars. A_{V_0} and θ_c (in degrees) are the fixed initial parameters for the models where a torus is incorporated. σ is the standard deviation for the variable on the left. A lower AIC (Akaike’s Information Criterion) value indicates a better model fit. The ‘Best fit’ model is the ‘Jet+Torus’ model for FRIs and FRIIs for which AIC is the minimum (see §3.5.2 in the text), the A_{V_0} and θ_c (in degrees) are the parameters corresponding to this fit.

Using the γ values derived as in Eq. 3 from the minimum and maximum values of R_c in our data set for each of the FRI and FRII populations and Eqs. 1 and 5 for L_o and R_c , we did a non-linear least squares fit to the data for both the FR populations separately. We used the Levenberg-Marquardt (LM) algorithm as implemented in the IDL package (the LMFIT routine). This routine gives the best-fit values of the free parameters, their standard deviations and the χ^2 goodness-of-fit. For the model-fitting we assumed the errors in the nuclear optical luminosity to be 50% (*e.g.*, Verdoes Kleijn et al. (2002)).

In order to quantify the goodness-of-fit of a particular model, we used the Akaike's information criterion (AIC). The AIC (Akaike 1974) is a likelihood criterion with an added penalty term corresponding to the complexity of the model, and measures the trade-off between model complexity/parsimony and goodness-of-fit. This criterion is used to compare different model-fits and is defined as :

$$AIC = -2 \ln(L) + 2 k \quad (\text{Burnham \& Anderson 2002})$$

where, $\ln(L)$ is the log likelihood function and is given by

$$\ln(L) = -(n/2) \{ \ln(2 \pi) + \ln(\text{SEE}/n) + 1 \}$$

where 'n' is the number of data-points, 'SEE' is the Standard error of estimate and 'k' is the number of parameters to be fit. Smaller AIC values indicate a better fit. We note that the goodness-of-fit criterion AIC, behaves in an inverse fashion to the χ^2 probability Q (Press et al. 1992).

For the 'Jet-only' model, L_{jet}^{int} is the only free parameter and the LM algorithm yields it's best fit value. For the 'Jet+Disk' model, both L_{jet}^{int} and L_{disk} are free parameters. The output of the algorithm turned out to be independent of the input seed values of these free parameters. The 'Jet+Disk+Torus' and the 'Jet+Torus' models have two additional parameters of the torus, *viz.*, A_{V_0} and θ_c . However, apart from the quality of the data, the fact that there are more than one "local minimum" for θ_c (discussed in §3.5.3) did not allow a robust estimation of all the parameters simultaneously. (The estimated values for θ_c strongly depended on the input seed value). We therefore adopted the procedure of manually varying the extinction A_{V_0} and torus half-opening angle θ_c and using the resulting AIC for each pair of (fixed) A_{V_0} and θ_c to infer the best fit.

Considering first the most general 'Jet+Disk+Torus' model to the fit the data, we chose a range of values for the torus parameters, A_{V_0} and θ_c , and estimated the best fit L_{jet}^{int} and L_{disk} using the LM algorithm. Results are tabulated in Table 6 for representative values, $A_{V_0} = 3$ and $\theta_c = 45^\circ$ (e.g., Barthel 1989). The resulting value of L_{disk} turned out to be insignificant in each case (see Table 6 and §3.5.3). We therefore further considered only the 'Jet+Torus' model which seemed more applicable to the data. For a given value of A_{V_0} we varied the θ_c from 0° through 90° and tabulated the resultant AIC. In Fig. 6 we plot the AIC against the torus half-opening angle for different fixed values of A_{V_0} .

As a next step, we fixed the torus half-opening angle θ_c to the value which had resulted in the minimum AIC (Fig. 6) – which is approximately the same for different values of A_{V_0} for each FR population, and let the A_{V_0} be the free parameter to be best-fitted by the LM algorithm. We found that the resultant A_{V_0} for the FRII objects was independent of the seed value whereas it depended on the initial value for the FRI objects. In this manner we estimated the "Best fit" 'Jet+Torus' model with values of A_{V_0} and θ_c which gave the least AIC. Table 6 lists the fitted parameters of the "Best fit" model for both the FR populations and Fig. 5 shows the best fit curves to each of the FR populations.

3.5.3. The results

The results of the model-fitting are given in Table 6. For the FRI population, the 'Jet-only' model is better than all the others. The 'Jet+Disk' model in fact yields a value for L_{disk} which is comparable to its standard deviation σ obtained from the fitting. Further, the 'Jet+Torus' model is best fit by parameters $A_{V_0} \approx 0.1$ and $\theta_c \approx 90^\circ$ which are equivalent to there being no torus.

For the FRII population as a whole, the results are less clear. Formally, the 'Jet-only' model has the least AIC, but the other models also yield comparable values. However, the L_{disk} that is obtained for 'Jet+Disk' and 'Jet+Disk+Torus' is unphysical. When only the broad-line objects among the FRIIs, *viz.*, the BLRGs and quasars are considered, the 'Jet+Disk' model was a better fit than the 'Jet-only' model (Table 6). This is consistent with the fact that the 'big blue bump' (attributed to the accretion disk) is observed in all these objects, and, in the framework of the Unified Scheme, the torus does not obscure the central regions in them. For the whole population, a larger number of data points in the regime where the disk is expected to be relatively most prominent, *viz.*, the intermediate R_c region, are required to derive a more robust quantitative value for L_{disk} since at large R_c the jet overwhelms the disk emission and at very small R_c the torus obscures it.

Given the unclear results of the model-fitting for the FRII population, we carry the procedure a bit further by contrasting the behaviour of the AIC for the FRIs and FRIIs in the 'Jet+Torus' model case. Figure 6 shows that the family of AIC plots for each population differ systematically from each other. The plots can be broadly divided into two parts. Below $\theta_c \approx 30^\circ$ the AIC drops for both the FRI and FRII population (shaded region in Fig. 6). This formally implies that the fit gets better for opening angles of the torus that are smaller than $\theta_c \approx 30^\circ$, but clearly is the result of the algorithm trying to fit the *entire* variation in L_o by torus obscuration *alone*. Above $\theta_c \approx 35^\circ$ the AIC declines again and reaches a minimum at angles close to 90° for the FRIs, consistent with there being no torus. For the FRIIs, the AIC does not decline appreciably above $\theta_c \approx 35^\circ$. In addition it shows a conspicuous minimum at $\theta_c \approx 37^\circ$.

Thus although simple model-fitting using the LM algorithm yielded ambiguous results for the FRIIs on the face of it, by rejecting the possibility that the entire variation in L_o is due to obscuration by a torus, we obtain model parameters that are broadly consistent with the predictions of the Unified Scheme. The model-fitting resulted in the

best θ_c roughly coinciding with the angle where the upper limits start appearing in FRII galaxies. The best A_{V0} turned out to ≈ 3 mag for the FRIIs at the best θ_c while for the FRIs, A_{V0} turned out to be ≈ 0 . We point out that the A_{V0} that we infer here is in the nature of a lower limit, since detection limits would exclude measured data points corresponding to higher values of A_{V0} . We find that the behaviour of FRI and FRII optical nuclei are distinctly different in that the model-fitting results are unambiguous for the FRIs while they are not so for the FRIIs, hinting at intrinsic differences between FRIs and FRIIs.

It may be recalled that the BL Lac objects taken by themselves show a flatter logarithmic distribution of L_o against R_c than would be expected from beaming alone (§3.3), and indeed model fitting just the BL Lacs gives the ‘Jet+Disk’ model to be the best one for them, with an implied L_{disk} of $3.3 \times 10^{22} \text{ W Hz}^{-1}$ (See Table 6). As was stated in §3.3, this is most likely to be due to the contaminating host galaxy luminosity mimicking emission from a disk. We note however, that unless values for their optical nuclei that are uncontaminated by the host galaxy are used, we cannot totally rule out an accretion disk in the BL Lacs alone, and therefore the implication that they may not be intrinsically similar to the FRI radio galaxies.

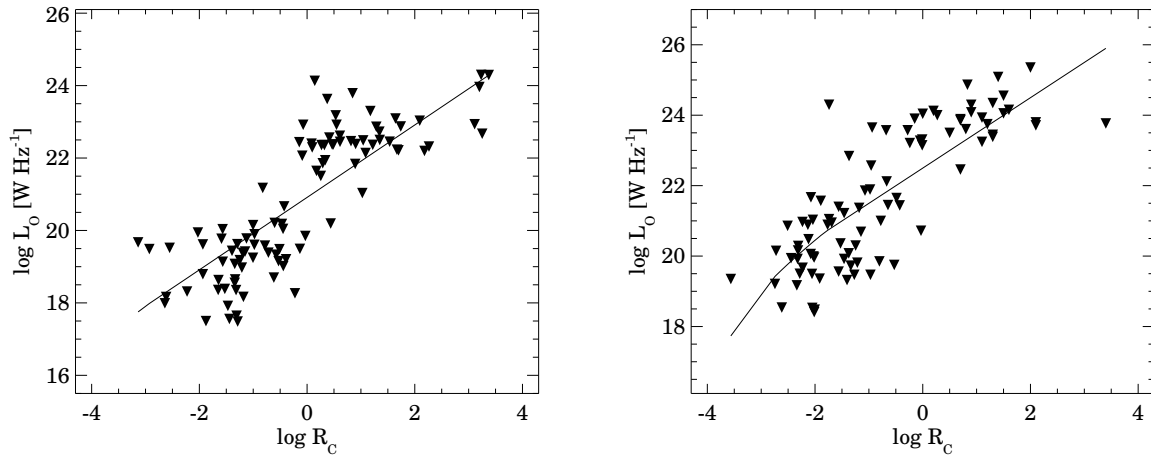


Fig. 5. Best fits to the FRI (left) and FRII (right) populations using only a ‘Jet+Torus’ model. Table 6 lists the model parameters.

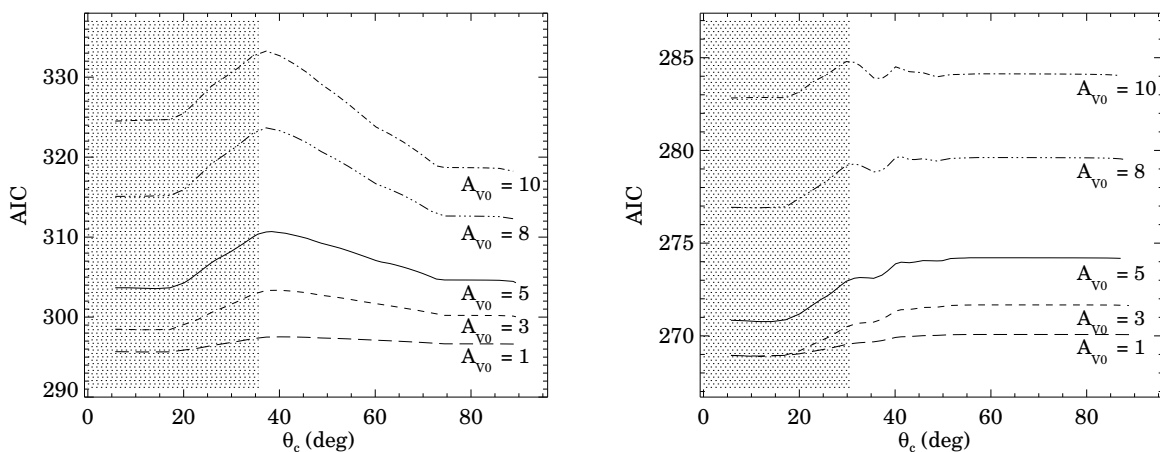


Fig. 6. AIC values for different initial A_{V0} plotted against torus opening angles θ_c (in degrees) for the FRI (left) and the FRII (right) populations for the ‘Jet+Torus’ model. For a given A_{V0} , AIC was estimated at 2° intervals of θ_c . The shaded area denotes the region where the model becomes unphysical; we disregard this regime in our discussion. In the physical regime, AIC is minimum at around 90° for the FRIs and 37° for the FRIIs.

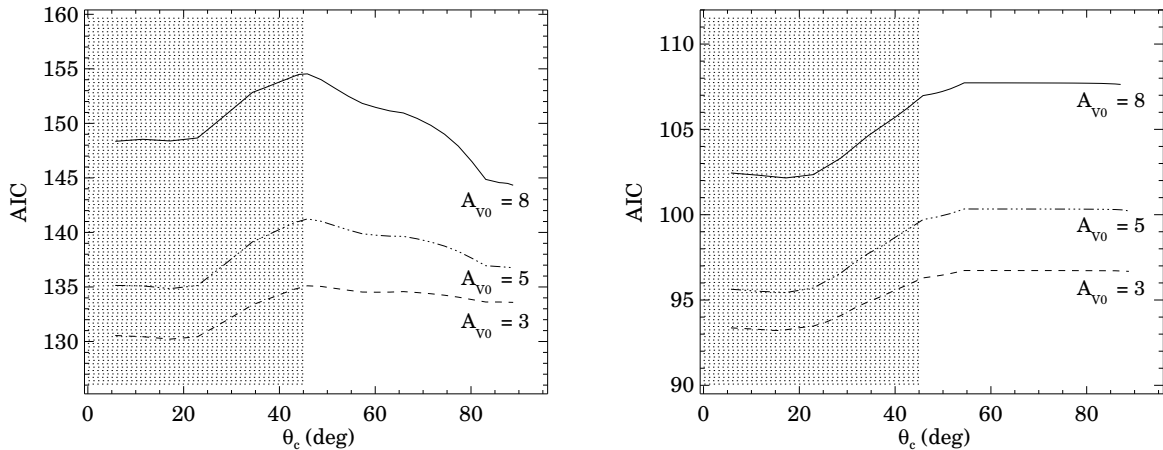


Fig. 7. AIC values for different initial A_{V0} plotted against torus opening angles θ_c (in degrees) for the matched subsamples of FRI (left) and the FRII (right) populations for the ‘Jet+Torus’ model. The shaded area denotes the region where the model becomes unphysical; we disregard this regime in our discussion. In the physical regime, AIC is minimum at around 90° for the FRIs while the case is not clear for FRIIs.

For the *smaller* matched subsamples of FRIs and FRIIs, the variation of AIC with θ_c (see Fig. 7) is broadly similar to that of their respective unrestricted samples. The only discernible difference for the ‘matched’ FRIIs is that the ‘AIC minimum’ observed at $\theta_c \approx 37^\circ$ for the whole sample, is now no longer prominent. However, this is not surprising in view of the fact that the ‘matched’ FRII objects are much fewer, especially at low radio core prominence values.

We considered the residuals for the model-fit on the R_c versus L_o data and examined them for any correlations with R_c and L_o . For both FRIs and FRIIs we find no correlation of the residuals with R_c and L_o . However, there seems to be a weak correlation for the BL Lacs considered alone. This may be reflective of the effects of ignoring the host galaxy luminosity when taking the optical core luminosity.

We note that while reliable quantitative results cannot be obtained using the current data because of the drawbacks with the sample, the approach and the results indicate that it is a good approach to derive various parameters if data for a rigorous and large sample are available. Better data would allow more parameters to be incorporated and controlled.

4. Discussion

We have investigated the nature of the newly discovered parsec-scale optical nuclei in radio galaxies in the context of the Fanaroff-Riley divide and the simple Unified Scheme. We have used the radio core-prominence parameter R_c as a statistical indicator of orientation with respect to our line of sight. We use a total of 54 FRI radio galaxies, 55 FRII radio galaxies, and further, 44 BL Lac objects (of FRI morphology) and 34 radio-loud quasars in the analysis, which includes statistical analysis and simple model-fitting.

We find that the optical core luminosity shows a strong correlation with radio core prominence R_c , or equivalently, orientation, for the 54 FRI radio galaxies but not for the 42 narrow-line FRII radio galaxies, which is confirmed by both non-parametric and parametric statistical tests. The strong correlation for the FRI radio galaxies suggests that their optical cores are orientation-dependent in the same way as the radio jets, and are likely to be of a similar non-thermal origin. The lack of correlation for the narrow-line FRII radio galaxies is suggestive of the presence of some obscuration (probably in the form of a dusty torus) of L_o which spoils any intrinsic correlation with R_c . We also note that there are more upper limits than detections of optical cores in the FRIIs.

Although the above correlation is very significant for the FRI galaxies, there is a significant amount of scatter that remains. Several FRI galaxies have been found to have extended (kpc-scale) dusty disks. For the 18 FRI galaxies studied here for which such disks have been seen, the nuclear optical luminosity significantly correlates with the orientation of this disk as measured by its apparent ellipticity. The orientation of these disks appear to bear no clear relation to the orientation of the AGN axis, however, as evidenced by the lack of any correlation with the core prominence R_c .

We find that the optical core luminosity of FRI and FRII radio galaxies taken along with 44 BL Lacs of FRI morphology and 34 radio-loud quasars respectively is strongly correlated with radio core prominence. We note that while the FRII radio galaxies alone did not show such a correlation, the broad-line FRIIs, *viz.*, the BLRGs and quasars taken together show a significant correlation of L_o with R_c , consistent with the idea that their obscuring tori is no

longer attenuating the optical nuclei in them. A multiple linear regression test with radio core prominence, redshift and extended radio luminosity shows that the $L_o - R_c$ correlation is the most significant for both the FR populations.

In order to understand the seemingly different functional forms obeyed by the data, we tried to fit some simple models to them. The most general model comprised of a relativistic optical synchrotron jet, an orientation-dependent thin accretion disk and an obscuring torus. We did not incorporate intrinsic variation in any of these components, nor the obscuring effects of an *extended* dusty disk. From the minimum and maximum values of R_c we derived the Lorentz factor γ to be ≈ 9 for the FRI population and ≈ 11.5 for the FRIIs, consistent with other inferences in the literature. The primary result from the model-fitting is that a relativistic beamed jet alone is a good fit to the variation in the optical cores of the FRI population. Although formally the ‘Jet+Torus’ model is also a good fit, the values of the opening angle and extinction derived are virtually equivalent to there being no torus ($A_V \approx 0$ and $\theta_c \approx 90^\circ$). For the FRII population, model-fitting indicates that formally the best fit is again a beamed synchrotron jet. But a beamed jet obscured by a torus with an inferred opening angle of $\approx 37^\circ$ is a comparable fit. Model-fitting the broad-line FRII sources by themselves implies that an optically luminous accretion disk contributes significantly along with the relativistic beamed jet.

These results are tentative to the extent that the objects that we have used constitute an eclectic sample. A more rigorous analysis requires construction of samples where the objects of a given FR population are chosen to be intrinsically similar in the framework of the Unified Scheme and from the same volume of space. Further, for the highly beamed objects, *viz.*, the quasars and much more so, the BL Lacs, measurements of their nuclei uncontaminated by the host galaxy should be used.

For the *smaller* matched subsamples of FRIs and FRIIs, where the extended radio luminosity and redshift are confined to a narrow range, a multiple linear regression test with the variables, R_c , z , L_{ext} shows that $L_o - R_c$ is still the strongest correlation while L_{ext} is no longer significant. The variation of AIC with θ_c is *broadly* similar to that for the unrestricted sample, validating our procedure and the *qualitative results* for the whole sample regarding the differences between FRIs and FRIIs. The only discernible difference for the matched FRIIs is that the ‘AIC minimum’ seen at $\theta_c \approx 37^\circ$ for the unrestricted sample, is now no longer prominent. However, this is probably due to much fewer ‘matched’ FRIIs, especially at low R_c .

The quantitative results of the model-fitting, on the other hand, can clearly be useful only when applied to a larger sample that is rigorously selected.

5. Conclusions

We use the radio core prominence R_c as a statistical indicator of orientation and find that the systematic differences between radio-loud AGN of the two Fanaroff-Riley types appear to also extend to their optical nuclei, in a manner that is consistent with the predictions of the simple Unified Scheme. We find that the behaviour of FRI and FRII optical nuclei are qualitatively different. We find that,

1. The luminosity of the parsec-scale optical nuclei in the FRI radio galaxies is orientation-dependent, while that in the FRII radio galaxies is not. This result is consistent with the idea that FRIIs contain an obscuring torus, (as required by the simple US) whereas there is no torus in the FRIs.
2. For the FRI radio galaxies, though the correlation with orientation is very significant, a significant amount of residual scatter remains. This may be due to obscuration from an *extended kpc-scale* dusty disk. The axis of this disk appears unrelated to the AGN axis. The residual scatter may also be due to intrinsic variation in the optical luminosity.
3. The optical core luminosity correlates significantly with R_c , or equivalently, orientation, for the FRI radio galaxies and BL Lacs of FRI morphology taken together – the FRI population. Our model-fitting suggests that a relativistically beamed optical jet gives the best fit.
4. For the FRII radio galaxies and radio-loud quasars taken together – the FRII population, the optical core luminosity again correlates significantly with R_c . Our model-fitting indicates that formally the best fit is again a beamed synchrotron jet. But a beamed jet obscured by a torus with an inferred opening angle close to 40° is a comparable fit, and is able to explain the contrasting behaviour of the FRI and FRII data.
5. The scatter in the $L_o - R_c$ correlation is likely to be a result of the spread in intrinsic AGN power.
6. Our model-fitting suggests that the luminosity of the intrinsic (*i.e.*, unbeamed) jet in the FRIIs is approximately an order of magnitude larger than for the FRIs, although this result needs to be confirmed using a rigorous sample.
7. The data for the broad-line FRIIs alone are best fit by a model that comprises of a relativistic jet and a thin optically thick disk, consistent with the presence of the ‘big blue bump’ in them.

The robustness of the above results are limited by the facts that (a) the “samples” used are eclectic, (b) the luminosity of the optical nuclei in the highly beamed objects is contaminated by the contribution of the host galaxy, and (c) there could be variability between the epochs of the optical and radio measurements. A robust analysis requires rigorous measurement of the optical luminosity as well as samples that are rigorously selected, with the objects of a given FR population chosen to be intrinsically similar in the framework of the Unified Scheme and from the same volume of space.

Acknowledgements. We are very grateful to Prof. Thriyambakam Krishnan for his scrutiny of our statistical tests and results, useful suggestions and extensive discussions.

References

Akaike, H. 1974, IEEE Transactions on Automatic Control, 19, 716

Antonucci, R. 1993, ARA&A, 31, 473

Baker, J. C., Hunstead, R. W., Kapahi, V. K., & Subrahmanyam, C. R. 1994, in The First Stromlo Symposium: The Physics of Active Galaxies. ASP Conference Series, Vol. 54, 1994, G.V. Bicknell, M.A. Dopita, and P.J. Quinn, Eds., p.195, 195–+

Barthel, P. D. 1989, ApJ, 336, 606

Baum, S. A., Zirbel, E. L., & O'Dea, C. P. 1995, ApJ, 451, 88

Becker, R. H., White, R. L., & Edwards, A. L. 1991, ApJS, 75, 1

Blandford, R. D. & Konigl, A. 1979, ApJ, 232, 34

Bridle, A. H. & Perley, R. A. 1984, ARA&A, 22, 319

Burnham, K. P. & Anderson, D. R. 2002, Model selection and multimodel inference: a practical information-theoretic approach. (Springer-Verlag, New York, NY.)

Capetti, A. & Celotti, A. 1999, MNRAS, 304, 434

Capetti, A., Celotti, A., Chiaberge, M., et al. 2002, A&A, 383, 104

Capetti, A., Fanti, R., & Parma, P. 1995, A&A, 300, 643

Cassaro, P., Stanghellini, C., Bondi, M., et al. 1999, A&AS, 139, 601

Chiaberge, M., Capetti, A., & Celotti, A. 1999, A&A, 349, 77

—. 2002, A&A, 394, 791

de Koff, S., Best, P., Baum, S. A., et al. 2000, ApJS, 129, 33

Falomo, R., Scarpa, R., & Bersanelli, M. 1994, ApJS, 93, 125

Fanaroff, B. L. & Riley, J. M. 1974, MNRAS, 167, 31P

Fomalont, E. B. & Bridle, A. H. 1978, AJ, 83, 725

Giovannini, G., Feretti, L., Gregorini, L., & Parma, P. 1988, A&A, 199, 73

Gregory, P. C. & Condon, J. J. 1991, ApJS, 75, 1011

Hardcastle, M. J., Alexander, P., Pooley, G. G., & Riley, J. M. 1996, MNRAS, 278, 273

Hardcastle, M. J. & Worrall, D. M. 1999, MNRAS, 309, 969

—. 2000, MNRAS, 314, 359

Impey, C. D. & Tapia, S. 1990, ApJ, 354, 124

Jannuzzi, B. T., Yanny, B., & Impey, C. 1997, ApJ, 491, 146

Jenkins, C. R. 1982, MNRAS, 200, 705

Kapahi, V. K. & Saikia, D. J. 1982, Journal of Astrophysics and Astronomy (ISSN 0250-6335), vol. 3, Dec. 1982, p. 465-483., 3, 465

Kapahi, V. K. & Shastri, P. 1987, MNRAS, 224, 17P

Kollgaard, R. I., Wardle, J. F. C., Roberts, D. H., & Gabuzda, D. C. 1992, AJ, 104, 1687

Kotilainen, J. K., Falomo, R., & Scarpa, R. 1998, A&A, 336, 479

Kuehr, H., Nauber, U., & Pauliny-Toth, I. I. K. 1979, A Catalogue of radio sources (Bonn: Max-Planck-Institut (MPI) fuer Radioastronomie, 1979)

Kuehr, H., Pauliny-Toth, I. I. K., Witzel, A., & Schmidt, J. 1981, AJ, 86, 854

Laing, R. A., Parma, P., de Ruiter, H. R., & Fanti, R. 1999, MNRAS, 306, 513

Laurent-Muehleisen, S. A., Kollgaard, R. I., Moellenbroek, G. A., & Feigelson, E. D. 1993, AJ, 106, 875

Laurent-Muehleisen, S. A., Kollgaard, R. I., Ryan, P. J., et al. 1997, A&AS, 122, 235

Ledlow, M. J. & Owen, F. N. 1996, AJ, 112, 9

Meier, D. L. 1999, ApJ, 522, 753

Mirabel, I. F. & Rodriguez, L. F. 1994, Nature, 371, 46

Morris, S. L., Stocke, J. T., Gioia, I. M., et al. 1991, ApJ, 380, 49

O'Dea, C. P., Barvainis, R., & Challis, P. M. 1988, AJ, 96, 435

Orr, M. J. L. & Browne, I. W. A. 1982, MNRAS, 200, 1067

Padovani, P. & Giommi, P. 1995, MNRAS, 277, 1477

Perlman, E. S. & Stocke, J. T. 1993, ApJ, 406, 430

Pica, A. J., Smith, A. G., Webb, J. R., et al. 1988, AJ, 96, 1215

Press, W. H., Flannery, B. P., Teukolsky, S. A., & Vetterling, W. T. 1992, Numerical Recipes in Fortran. (Cambridge University Press.)

Prestage, R. M. & Peacock, J. A. 1988, MNRAS, 230, 131

Rector, T. A. & Stocke, J. T. 2001, AJ, 122, 565

Simpson, C. 1996, *Vistas in Astronomy*, 40, 57

Slee, O. B., Siegman, B. C., & Perley, R. A. 1989, *Australian Journal of Physics*, 42, 633

Smith, E. P. & Heckman, T. M. 1990, ApJ, 348, 38

Spangler, S. R. & Sakurai, T. 1985, ApJ, 297, 84

Urry, C. M. & Padovani, P. 1995, PASP, 107, 803

Verdoes Kleijn, G. A., Baum, S. A., de Zeeuw, P. T., & O'Dea, C. P. 1999, AJ, 118, 2592

—. 2002, AJ, 123, 1334

Vermeulen, R. C. & Cohen, M. H. 1994, ApJ, 430, 467

Veron-Cetty, M. P. & Veron, P. 1998, *VizieR Online Data Catalog*, 7207, 0

Waggett, P. C., Warner, P. J., & Baldwin, J. E. 1977, MNRAS, 181, 465

Webb, J. R., Smith, A. G., Leacock, R. J., et al. 1988, AJ, 95, 374

Wills, B. J., Wills, D., Breger, M., Antonucci, R. R. J., & Barvainis, R. 1992, ApJ, 398, 454

Xu, C., Baum, S. A., O'Dea, C. P., Wrobel, J. M., & Condon, J. J. 2000, AJ, 120, 2950

Zirbel, E. L. & Baum, S. A. 1995, ApJ, 448, 521